Disponible en ligne sur www.sciencedirect.com
ScienceDirect
Cancer/Radiothérapie 12 (2008) 800–808
CANCER RADIOTHÉRAPIE
http://france.elsevier.com/direct/CANRAD/

Original article

A phantom study of the accuracy of CT, MR and PET image registrations with a block matching-based algorithm

Étude sur fantôme de la précision d'un algorithme de recalage par blocs pour des images TDM, IRM et TEP

A. Isambert [a,*], G. Bonniaud [a], F. Lavielle [a], G. Malandain [b], D. Lefkopoulos [a]

[a] *Service de physique médicale, institut Gustave-Roussy, 39, rue Camille-Desmoulins, 94805 Villejuif, France*
[b] *Asclépios, institut national de recherche en informatique et automatique, 2004, route des Lucioles, 06902 Sophia-Antipolis, France*

Received 14 November 2007; received in revised form 25 April 2008; accepted 30 April 2008
Available online 20 June 2008

Abstract

Purpose. – The aim of the present study was to quantitatively assess the performance of a block matching-based automatic registration algorithm integrated within the commercial treatment planning system designated ISOgray™ from Dosisoft. The accuracy of the process was evaluated by a phantom study on computed tomography (CT), magnetic resonance (MR) and positron emission tomography (PET) images.

Materials and methods. – Two phantoms were used to carry out this study: the cylindrical Jaszczak® phantom and the anthropomorphic Liqui-Phil™ Head Phantom (the Phantom Laboratory), containing fillable spheres. External fiducial markers were used to quantify the accuracy of 41 CT/CT, MR/CT and PET/CT automatic registrations with images of the rotated and tilted phantoms.

Results. – The study first showed that a cylindrical phantom was not adapted for the evaluation of the performance of a block matching-based registration software. Secondly, the Liqui-Phil™ Head Phantom study showed that the algorithm was able to perform automatic registrations of CT/CT and MR/CT images with differences of up to 40° in phantom rotation and of up to 20–30° for PET/CT with accuracy below the image voxel size.

Conclusion. – The study showed that the block matching-based automatic registration software under investigation was robust, reliable and yielded very satisfactory results. This phantom-based test can be integrated into a periodical quality assurance process and used for any commissioning of image registration software for radiation therapy.

Résumé

Objectif de l'étude. – Évaluer quantitativement, à l'aide de fantômes, la précision d'un algorithme de recalage automatique par blocs, intégré dans le système de planification de traitement ISOgray™ (Dosisoft), pour des images acquises par tomodensitométrie (TDM), résonance magnétique (IRM) et tomographie à émission de positons (TEP).

Matériel et méthodes. – Deux fantômes contenant des sphères remplissables ont été utilisés au cours de cette étude : le fantôme cylindrique de Jaszczak® et le fantôme anthropomorphique Liqui-Phil™ Head (the Phantom Laboratory). Des repères externes ont permis de quantifier la précision du recalage automatique d'images TDM/TDM, IRM/TDM, TEP/TDM pour 41 configurations, avec les fantômes tournés ou inclinés par rapport à une position de référence.

Résultats. – La première étude a montré qu'un fantôme cylindrique n'était pas adapté pour évaluer les performances d'un algorithme de recalage par blocs. Deuxièmement, l'étude menée à l'aide du fantôme Liqui-Phil™ Head a montré que la précision des recalages était inférieure aux dimensions des voxels des images utilisées, pour des différences en rotation allant jusqu'à 40° pour les recalages TDM/TDM et IRM/TDM et d'un maximum de 20 à 30° pour les recalages TEP/TDM.

* Corresponding author.
E-mail address: aurelie.isambert@igr.fr (A. Isambert).

1278-3218/$ – see front matter © 2008 Elsevier Masson SAS. All rights reserved.
doi:10.1016/j.canrad.2008.04.009

Conclusion. – L'étude a montré que l'algorithme de recalage automatique d'images fondé sur le recalage par blocs était robuste, fiable et donnait des résultats très satisfaisants sur fantôme. Les tests proposés dans cette étude peuvent être intégrés dans un processus de contrôle qualité périodique et utilisés à la réception de tous nouveaux logiciels de recalage d'images pour la radiothérapie.

Keywords: Multimodality image registration; Radiation therapy; Quality assurance; Block matching; Phantom study

Mots clés : Recalage d'images multimodalités ; Radiothérapie ; Assurance qualité ; Recalage par blocs ; Étude sur fantôme

1. Introduction

The development of ever more sophisticated radiation therapy techniques such as intensity modulated radiation therapy (IMRT) has led to the use of high dose distribution gradients allowing the delivery of greater doses to the target volume, while sparing nearby organs at risk. This has emphasized the increasing need for accurately delineated structures of interest. Although computed tomography (CT) images remain the gold standard for planning most radiotherapy sessions in daily clinical practice, since this is the only imaging modality able to provide information in terms of electronic density for dose calculation, the importance of additional information provided by magnetic resonance imaging (MRI) and positron emission tomography (PET) images has been highlighted [4,6,13,18–20,26]. These modalities are now widely used as a second source of information to help physicians delineate volumes of interest. Fusion of the coregistered images from different modalities provides additional information, thereby reducing uncertainties in image interpretation.

Two main items should be considered regarding registration techniques: the nature of the registration and the nature of the transformation, as described by Maintz and Viergever [15]. The registrations can be extrinsic, that is based on a foreign object introduced into the image space, such as a stereotactic frame, skin markers, or fiducial markers that are screwed into the patient's skull or intrinsic, that is based on image information. Registration methods can be classified into two main categories: the geometric method based on the detection of geometric features as points or lines and the iconic method based on the voxel property. The nature of the registration transformation can be rigid, affine, projective or nonlinear [15]. Multimodality image registration is a complex process because of the difficulty to correlate information of a different nature (anatomic or functional) and with different characteristics (spatial resolution, contrast...). The image registration process is prone to errors that can lead to patient treatment errors consequently, the accuracy of image registration must be assessed and verified [3,17].

Several teams have addressed this issue using different techniques. The most realistic way to assess the accuracy of a registration is to use patient images on which anatomical landmarks [23,24] or external markers [1,8,27,28] can be identified. Another method consists in using phantoms like the Hoffman phantom [5,25,28] or anthropomorphic head phantoms like those described by Mutic et al. and Lavely et al. [12,17] with additional external or internal markers. With this approach, multimodal image (CT, MR and PET) acquisitions can be completed with the same phantom filled with the appropriate contrast agents (iodine, copper sulfate or gadolinium and ^{18}F-FDG, respectively). A third approach consists in using simulated data for the brain [9,11,29]: MRI, PET and SPECT images can be calculated. Known displacements can be applied to the images and then compared to the values calculated by the automatic registration algorithm which is to be tested.

Quality assurance of a multimodality image registration process is highly recommended for general commissioning and periodical testing by the American Association of Physicists in Medicine (AAPM TG 53 report [7]) and also in technical report or booklet from the International Atomic Energy Agency (IAEA) [10] and the European Society for Therapeutic Radiology and Oncology (ESTRO) [16]. Most of the studies evaluating the performance of automatic registration software in the literature concern mutual information-based algorithms [8,12,14,29]. In our study, the automatic registration algorithm to be tested is a block matching-based algorithm [21] integrated within the commercial treatment planning system (TPS) designated ISOgray™ from Dosisoft. The algorithm is described in the Section 2 as well as the two phantoms used to accomplish this study. Then, we first demonstrate through qualitative evaluation using the Jaszczak® phantom, how important it is to select the appropriate phantom for the kind of algorithm to be tested. Secondly, using the Liqui-Phil™ Head Phantom (the Phantom Laboratory), we quantitatively evaluate the performance of the block matching-based algorithm.

2. Materials and methods

As image quality directly affects the ability to identify and delineate target volumes and surrounding critical structures for radiation treatment planning, the imaging performance of CT, MR and PET scanners is tested periodically in our institution to verify the signal to noise ratio, uniformity, spatial resolution and distortions (especially for MR images), as part of the quality assurance program. These tests are a prerequisite for the quantitative assessment of image registration software.

The purpose of this work was to assess the performance of the automatic registration software "Baladin" which is a block matching-based algorithm (http://www-sop.inria.fr/epidaure/software/Baladin) (Fig. 1). This method is very similar to the iterative closest point algorithm (ICP [2]), which consists in extracting feature points in the reference images and in images to be registered (called floating images) and in repeating the following steps until convergence:

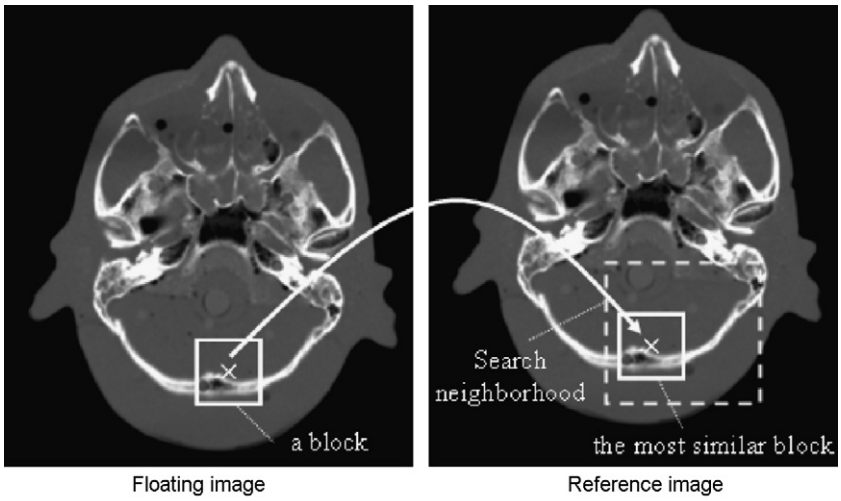

Fig. 1. Principle of the block matching-based algorithm.
Fig. 1. Principe de l'algorithme de recalage par blocs.

- to pair each feature point of the floating image with the closest feature point in the reference image;
- to compute the transformation that will best superimpose the paired points;
- to apply this transformation to the feature points of the floating image.

The pairing may have changed after applying the transformation; repeating these three steps may therefore allow one to find a better transformation. Unlike the ICP algorithm, feature points are not extracted in the block matching algorithm. Sub-images (blocks) are considered in the floating image and are paired with the most similar sub-image in the reference image. The computed transformation is the one that will best superimpose the centers of the paired sub-images. Only the blocks with the largest standard deviation are considered for pairing. Once the pairings are calculated, the transformation is computed using least trimmed squares so that outliers can be detected and removed from the transformation estimation.

This algorithm calculates rigid transformation which can be written in the following manner:

$$T(\alpha) = R\alpha + t \quad (1)$$

with T being the transformation to be applied to the point α, R the rotation matrix (3×3 matrix) and t, the translation vector.

The algorithm was integrated within the TPS ISOgray™ and it can be used through two different modules: a fully automatic one with no intervention from the user and an advanced one in which the user can modify three parameters regarding the degree of pyramid [21], the number of iterations and a threshold to eliminate noise in the images.

In the present work, two series of tests were performed on the registration algorithm, using the fully automatic module, to test its performance in registering CT, MR and PET images.

2.1. Assessment methodology using a Jaszczak® phantom

The first series of tests were achieved with a Jaszczak® cylindrical phantom with six external capillary tubes (fiducial markers) and five spheres (four fillable spheres and one "cold" sphere). The phantom, tubes and spheres were filled with contrast products for CT and MR images (iodine and gadolinium, respectively). Several series of images were acquired with parameters as close as possible to those used in clinical practice:

- CT images on a Siemens Sensation Open 20 scanner (2 mm slice thickness) with:
  - the phantom in a "reference" position (Fig. 2a),
  - the phantom rotated around the craniocaudal axis (Fig. 2b),
  - the phantom tilted (Fig. 2c);
- MR images on a General Electric Signa Excite 1.5T scanner (head coil, sequence AX3D SPGR 3 mm, T1-weighted axial images) with the phantom in the "reference" position.

The performance of the automatic registration software was qualitatively assessed by two medical physicists by visual inspection of several MR/CT image registrations using a checkerboard rendered image display.

2.2. Assessment methodology with the Liqui-Phil™ Head phantom

The second series of tests were accomplished with an anthropomorphic phantom which is similar to those already used by Mutic et al. and Lavely et al. [12,17]: the Liqui-Phil™ Head Phantom (the Phantom Laboratory), has four external capillary tubes (fiducial markers) and two fillable spheres. The tubes and spheres were filled with contrast products: iodine, gadolinium and ^{18}F-FDG. The phantom itself was filled with water, copper

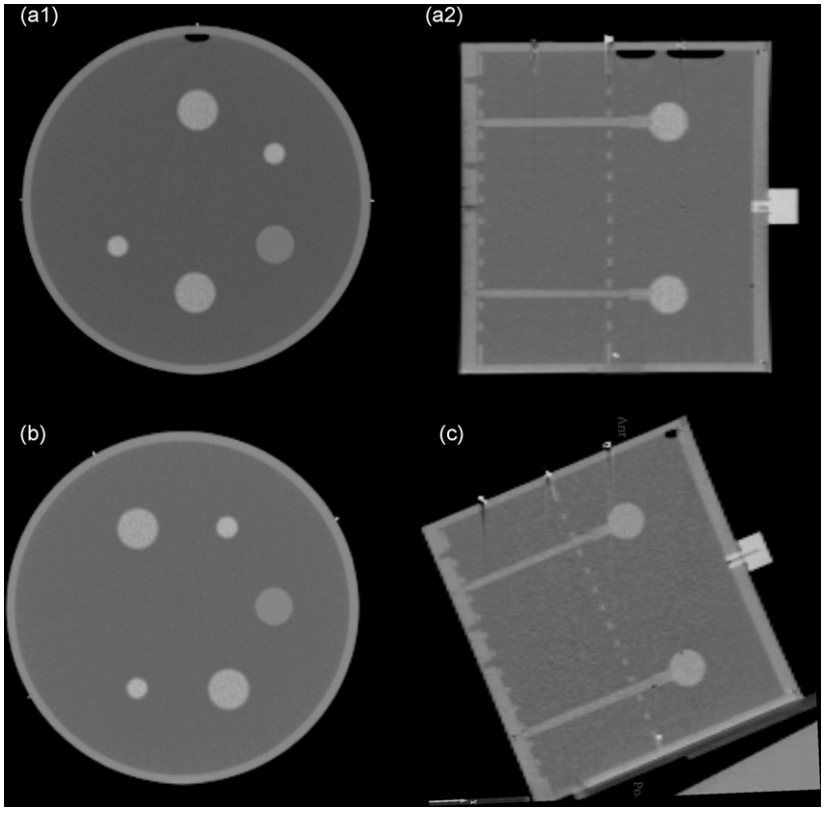

Fig. 2. CT images of the Jaszczak® phantom in (a) the reference position (a.1: axial view, a.2: sagittal view) and (b) rotated around the craniocaudal axis; (c) tilted (rotation around the left–right axis).
Fig. 2. Images TDM du fantôme Jaszczak® dans (a) la position de référence (a.1 : vue axiale ; a.2 : vue sagittale) et (b) une rotation autour de l'axe craniocaudal ; (c) incliné (rotation autour de l'axe gauche–droite).

sulfate and ^{18}F-FDG. Sixteen series of images were acquired with parameters as close as possible to those used in clinical practice:

- CT images on a Siemens Sensation Open 20 scanner (2 mm slice thickness) with:
  - the phantom in a "reference" position (Fig. 3a),
  - the phantom rotated around the left–right axis (x-axis) (Fig. 3b), the rotation angles related to the "reference" position were: 10, 20, 30 and 40°,
  - the phantom rotated around the craniocaudal axis (y-axis) (Fig. 3c), the rotation angles related to the "reference" position were: 10, 20, 30, 45 and 90°,
  - the phantom rotated around the anteroposterior axis (z-axis) (Fig. 3d), the rotation angles related to the "reference" position were: 10, 20, 30 and 40°;
- T1-weighted MR images on a General Electric Signa Excite 1.5T scanner (head coil, sequence AX3D SPGR 3 mm, T1-weighted axial images) were acquired with the phantom in the "reference" position;
- PET images on an Ecat Exact HR$^+$ camera (Siemens Molecular Imaging) were acquired with the phantom in the "reference" position (two bed positions, seven minute-emission scan and three minute-transmission scan [Germanium source] per bed position).

The 3D data were rebinned to a 2D dataset using Fourier Rebinning (FORE) followed by reconstruction using attenuation-weighted ordered subset expectation maximization (OSEM).

The following registration combinations were tested (floating images/reference images): CT/CT (rotated or tilted), MR/CT ("reference position", rotated or tilted), PET/CT ("reference position", rotated or tilted).

In this second series of tests, a quantitative assessment method, similar to the one described by Turkington et al. [25], was used. This method consisted in four steps:

- the positions of each external fiducial marker attached to the surface of the phantom were manually recorded on the two original sets of images before registration with (β_i) the coordinates of the markers in the set of reference images and (γ_i) the coordinates in the set of floating images;
- the two sets of images were automatically registered: the corresponding transformation matrix, T_{auto}, was recorded;
- the transformation matrix T_{auto} was applied to the coordinates of the markers on the floating images before registration ($T_{\text{auto}}[\gamma_i]$);
- the deviation δ between the coordinates was calculated:

$$\delta = |\beta_i - T_{\text{auto}}(\gamma_i)| \quad (2)$$

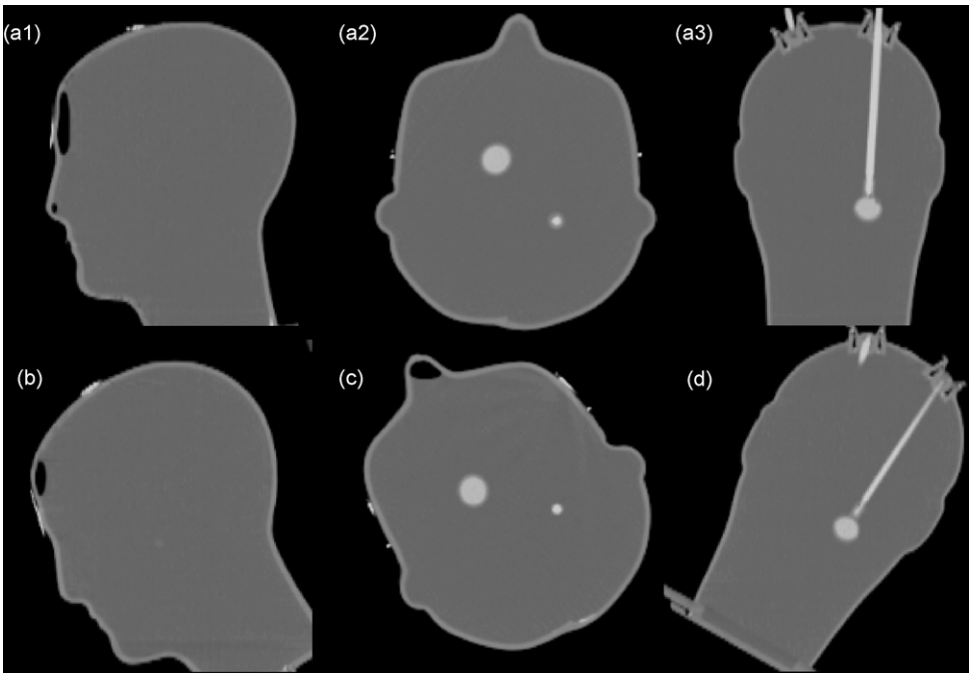

Fig. 3. CT images of the Liqui-Phil™ Head Phantom in (a) the reference position (a.1: sagittal view, a.2: axial view, a.3: coronal view) and rotated around (b) the left–right axis; (c) the craniocaudal axis; (d) the anteroposterior axis.
Fig. 3. Images TDM du fantôme Liqui-Phil™ Head dans (a) la position de référence (a.1 : vue sagittale ; a.2 : vue axiale ; a.3 : vue coronale) et une rotation autour de (b) l'axe gauche–droite ; (c) l'axe craniocaudal ; (d) l'axe antéropostérieur.

The mean deviation was calculated for each direction (δx, δy, δz).

2.3. Uncertainty in marker localization due to operator interaction

When considering the second series of tests, the deviation δ, calculated to evaluate the accuracy of the registration process, took into account two potential errors: possible mismatching due to the registration algorithm itself and uncertainty in localizing the markers due to operator interaction. The uncertainty in manually localizing the markers was evaluated for CT, MR and PET images separately. In order to do so, each of the four markers was manually localized 12 times by the same operator on CT, MR and PET images and the mean directional standard deviation was calculated for each imaging modality.

3. Results

The registrations were computationally efficient: the time required to run the algorithm was inferior to one minute, without any intervention from the user.

3.1. Results related to the tests performed with Jaszczak® phantom

Several sets of MR and CT images of the Jaszczak® phantom (with CT images as reference images) were automatically registered. The image registration results were visually checked by verifying the superimposition of the external markers and also the overlapping of the internal spheres on both modalities, as recommended by Mutic et al. [17]. The automatic registration algorithm failed to match MR images with CT images of the Jaszczak® phantom with a rotation angle greater than 10° or with a tilted angle greater than 20°. These results indicated that the cylindrical Jaszczak® phantom, because of its too regular shape and design, was not adapted for assessing the performance of a block matching-based algorithm. Consequently, a second series of tests was performed with an anthropomorphic head phantom.

3.2. Results related to the tests performed with Liqui-Phil™ Head phantom

The automatic registration process was tested with the Liqui-Phil™ Head phantom and the three imaging modalities using the same algorithm based on the block-matching principle. Forty-one combinations of CT/CT (13 combinations), MR/CT (14 combinations) and PET/CT (14 combinations) image automatic registration were verified. The deviation between the marker coordinates was calculated for each couple of images for the three directions x, y, z which correspond to the left–right axis, craniocaudal axis and anteroposterior axis, respectively.

3.2.1. CT/CT image registrations

The CT image voxel size was $v_x = 1.09$ mm, $v_y = 2$ mm, $v_z = 1.09$ mm. The mean deviation (δ_{mean}) of the different CT/CT image registrations was below the voxel size for 12 rotation configurations: rotations around the left–right axis (10, 20, 30, 40°), around the craniocaudal axis (10, 20, 30, 45°) and the anteroposterior axis (10, 20, 30, 40°). The results of these satisfactory automatic registrations, which correspond to a mean deviation that is close to the voxel size, are presented in Fig. 4, for the

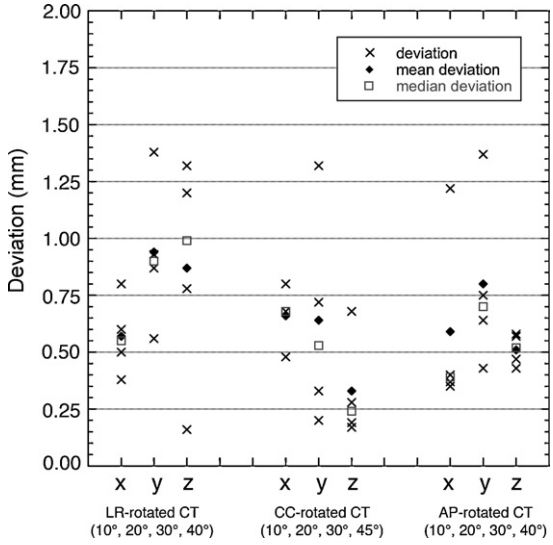

Fig. 4. Results of the CT/CT image registrations (voxel size: $v_x = 1.09$ mm, $v_y = 2$ mm, $v_z = 1.09$ mm). The three directions x, y, z correspond to the left–right, craniocaudal and anteroposterior axis, respectively. LR-rotated CT, CC-rotated CT, AP-rotated CT are CT images of the head phantom rotated around the left–right axis, the craniocaudal axis and anteroposterior axis, respectively.

Fig. 4. Résultats des recalages TDM/TDM (taille des voxels : $v_x = 1{,}09$ mm, $v_y = 2$ mm, $v_z = 1{,}09$ mm). Les trois directions x, y, z correspondent aux axes gauche–droite, craniocaudal et antéropostérieur, respectivement. *LR-rotated CT, CC-rotated CT, AP-rotated CT* sont les images TDM du fantôme en rotation autour de l'axe gauche–droite, l'axe craniocaudal et l'axe antéropostérieur, respectivement.

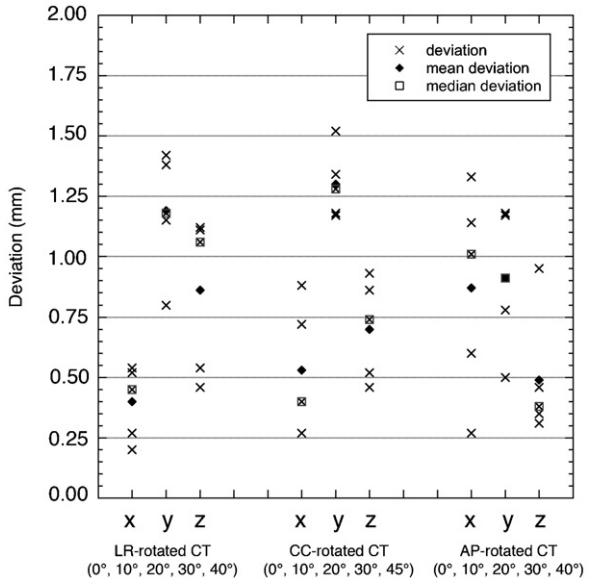

Fig. 5. Results of the MR/CT image registrations (voxel size [CT]: $v_x = 1.09$ mm, $v_y = 2$ mm, $v_z = 1.09$ mm, voxel size [MR]: $v_x = 0.47$ mm, $v_y = 3$ mm, $v_z = 0.47$ mm). The three directions x, y, z correspond to the left–right, craniocaudal and anteroposterior axis, respectively. LR-rotated CT, CC-rotated CT, AP-rotated CT are CT images of the head phantom rotated around the left–right axis, the craniocaudal axis and anteroposterior axis, respectively.

Fig. 5. Résultats des recalages IRM/TDM (taille des voxels [TDM] : $v_x = 1{,}09$ mm, $v_y = 2$ mm, $v_z = 1{,}09$ mm, taille des voxels (IRM) : $v_x = 0{,}47$ mm, $3\text{ mm} = v_y$, $v_z = 0{,}47$ mm). Les trois directions x, y, z correspondent aux axes gauche–droite, craniocaudal et antéropostérieur respectivement. *LR-rotated CT, CC-rotated CT, AP-rotated CT* sont les images du fantôme en rotation autour de l'axe gauche–droite, l'axe craniocaudal et l'axe antéropostérieur respectivement.

three directions x, y, z. The algorithm only failed to match the CT images of the phantom in the reference position with the CT images of the phantom rotated around the craniocaudal direction at an angle of 90°.

3.2.2. MR/CT image registrations

The MR image voxel size was $v_x = 0.47$ mm, $v_y = 3$ mm, $v_z = 0.47$ mm. Thus, the dimensions to be considered as acceptability criteria for registering the MR/CT image were the maximum voxel size of the two modalities ($\delta x = 1.09$ mm, $\delta y = 3$ mm, $\delta z = 1.09$ mm). The MR/CT automatic registration process was successful for 13 combinations: rotations around the left–right axis (0, 10, 20, 30, 40°), around the craniocaudal axis (10, 20, 30, 45°) and the anteroposterior axis (10, 20, 30, 40°). The results of the successful automatic registrations are presented in Fig. 5, for the three directions x, y, z. The algorithm only failed to match the MR images of the phantom in the reference position with the CT images of the phantom rotated around the craniocaudal direction at an angle of 90°.

3.2.3. PET/CT image registrations

The PET image voxel is isotropic and equal to 2.42 mm. The results for the satisfactory PET/CT automatic registrations are presented in Fig. 6. The PET/CT automatic registration process was satisfactory when the CT images of the phantom were rotated around the left–right axis or around the craniocaudal axis up to an angle of 20°, or rotated around the anteroposterior axis up to an angle of 30°. To appraise the amplitude of the deviation for the unsatisfactory configurations, the results of all the tested configurations are presented in Table 1. We observed a clinically unacceptable mean deviation attaining 27.29 mm. The algorithm totally failed to match the PET images of the phantom in the reference position with the CT images of the phantom rotated around the craniocaudal direction at an angle of 90°.

Table 1
Mean deviation of the markers for the PET/CT image registrations with the anthropomorphic head phantom
Tableau 1
Déviation moyenne des repères pour les images TEP/TDM recalées

Floating/reference images	δx_{mean} (mm)	δy_{mean} (mm)	δz_{mean} (mm)
PET/CT ref	1.27	2.42	2.35
PET/CT LR-rot10°	0.60	2.01	1.64
PET/CT LR-rot20°	0.64	1.36	0.98
PET/CT LR-rot30°[a]	0.74	6.87	1.06
PET/CT LR-rot40°[a]	8.17	27.29	9.89
PET/CT CC-rot10°	1.40	1.71	2.31
PET/CT CC-rot20°	1.86	2.12	1.01
PET/CT CC-rot30°[a]	8.50	7.18	7.87
PET/CT CC- rot45°[a]	12.66	10.04	12.34
PET/CT AP-rot10°	0.60	2.28	2.06
PET/CT AP-rot20°	1.97	1.96	2.18
PET/CT AP-rot30°	0.85	2.51	1.52
PET/CT AP-rot40°[a]	7.74	21.25	14.59

LR, CC and AP means rotations of the CT images around the left–right axis, craniocaudal axis and anteroposterior axis, respectively.

[a] Nonsatisfactory results.

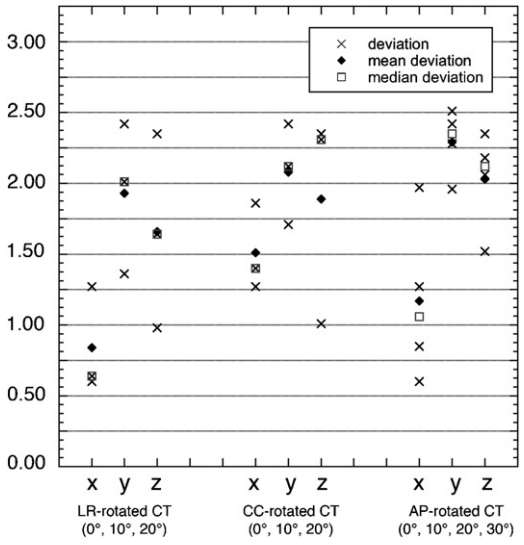

Fig. 6. Results for the PET/CT image registrations (voxel size [CT]: v_x =1.09 mm, v_y = 2 mm, v_z = 1.09 mm, voxel size [PET]: $v_x = v_y = v_z$ = 2.42 mm). The three directions *x*, *y*, *z* correspond to the left–right, craniocaudal and anteroposterior axis, respectively. LR-rotated CT, CC-rotated CT, AP-rotated CT are CT images of the head phantom rotated around the left–right axis, the craniocaudal axis and anteroposterior axis, respectively.

Fig. 6. Résultats des recalages TEP/TDM (taille des voxels [TDM] : v_x =1,09 mm, v_y = 2 mm, v_z = 1,09 mm, taille des voxels [TEP] : $v_x = v_y = v_z$ = 2,42 mm). Les trois directions *x*, *y*, *z* correspondent aux axes gauche–droite, craniocaudal et antéropostérieur, respectivement. *LR-rotated CT, CC-rotated CT, AP-rotated CT* sont les images du fantôme en rotation autour de l'axe gauche–droite, l'axe craniocaudal et l'axe antéropostérieur, respectivement.

3.3. Uncertainty in marker localization due to operator interaction

The uncertainty in manually localizing the markers was evaluated by recording the coordinates of each marker on CT, MR and PET images separately, 12 times and by calculating the corresponding mean directional standard deviations. According to the results presented in Table 2, the maximum uncertainty was mainly in the *y* direction (S.D.$_y$) which corresponds to the craniocaudal direction. It is in fact more difficult localize the markers accurately in this direction due to the slice thickness (2, 3 and 2.42 mm for CT, MR and PET images, respectively). This should be taken into account when analyzing the results presented in Figs. 4–6 and Table 1.

Table 2
Evaluation of the uncertainty in the manual localization of the markers on CT, MR and PET images
Tableau 2
Évaluation de l'imprécision de la localisation manuelle des repères sur les images TDM, IRM et TEP (S.D. est l'écart type directionnel moyen pour 12 mesures)

Modality	S.D.$_x$ (mm)	S.D.$_y$ (mm)	S.D.$_z$ (mm)
CT	0.22	0.51	0.20
MRI	0.21	0.46	0.19
PET	0.49	0.65	0.67

S.D. is the mean directional standard deviation for 12 measurements.

4. Discussion

One way to assess the accuracy of a complete registration process is to use patient images on which anatomical or external markers can be identified [1,8,23,24,27,28]. However, the use of patient images poses several problems. The first issue is acquiring a large set of CT, MR and PET images of the same patient with identifiable markers. It is noteworthy that anatomical landmarks are not always visible on these three modalities, consequently the major issue is the lack of ground truth. To be certain that identification is possible, external markers must be placed on the patient's skin which excludes the possibility of a retrospective study. Another approach was investigated by Pappas et al. to test CT/MR registration without using fiducial markers [22]: the technique described was based on the segmentation of cortical bone structures in CT and MR images. However, this technique requires the use of a dedicated automatic threshold selection method and cannot be applied to PET images. Consequently, the assessment of automatic registration software is mainly based on the use of phantoms. There are two consequences of using such objects to perform the tests:

- the phantom is not as heterogeneous as a human body even if some spheres are placed inside it to simulate tumors. For example, in our case, this can be a drawback for the block matching-based registration algorithm because image variance is less marked than in real bodies. Thus, the difficulty in achieving image registration might be increased;
- the use of a phantom does not allow for possible organ motion or changes in the shape of organs between two examinations or even during the acquisition of a series of images. For instance, there was no blurring due to breathing during the acquisition of PET images.

However, phantom studies allow one to verify the absence of systematic biases and to achieve an initial assessment of the performance and accuracy of the automatic registration algorithm. Phantom images can also be used to compare different algorithms.

A software quality assurance program based on a phantom study can therefore be an alternative to the use of patient images for an initial assessment. However, it should be borne in mind that the choice of the phantom may influence the results according to the nature of the algorithm tested. Indeed, in the present work, when we considered the series of tests performed with the Jaszczak® phantom, the automatic registration software seemed to handle images with different rotations around an axis that is parallel to the slice thickness (craniocaudal axis) less efficiently, which one might not have imagined intuitively. The algorithm used for automatic registration in our study is a block matching-based algorithm. Consequently, if two sets of images of the same phantom scanned in a reference position (Fig. 7a) and in a position rotated around the craniocaudal axis (Fig. 7b) have to be registered, a phantom with a cylindrical geometry may disturb the algorithm. Fig. 7 shows an example of the problem caused by a cylindrical phantom. During the registration process, when the algorithm analyzed the information contained in the two

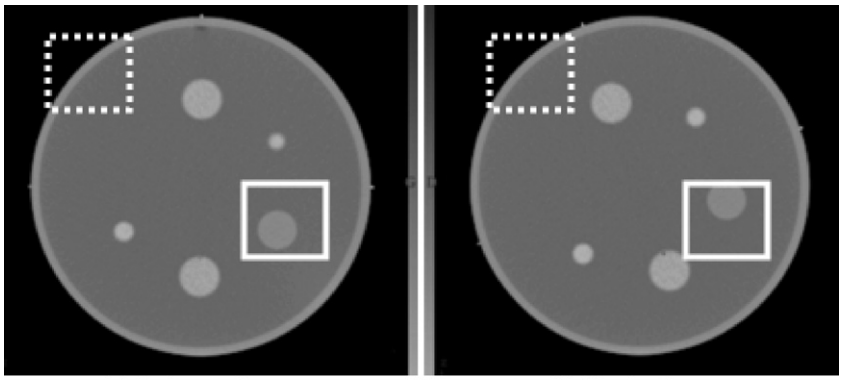

Fig. 7. Description of the problem induced by a phantom with a cylindrical geometry when testing a block matching-based registration algorithm.
Fig. 7. Description du problème induit par un fantôme avec une géométrie cylindrique lors de l'essai de l'algorithme de recalage par blocs.

windows (blocks) with dash lines and full lines, it found contradictory information: the information remained unchanged at the periphery of the phantom (dash-line windows) signifying an identity transformation matrix and was different inside the phantom (full-line windows) signifying a non identity transformation matrix. Most of the pairings generated by the algorithm consistently indicated the identity transformation matrix, while only a small number of them, built with blocks that contained the internal spheres, disagreed with this transformation. Due to the robust nature of the transformation calculation, they were subsequently considered as outliers and then discarded from this calculation. Consequently, given the kind of algorithm used, a cylindrical phantom with a too regular shape and design was not adapted for testing its performance.

These considerations explain why a second series of tests were carried out with the Liqui-Phil^{TM} Head Phantom, whose shape is more similar to a human being. The block matching-based algorithm yielded very satisfactory results for the CT/CT and MR/CT registrations. The algorithm failed only when CT images of the phantom were rotated around the craniocaudal axis at an angle of 90°. Regarding PET/CT image registration, the results seemed less satisfactory. The fact that CT and PET images are totally different in nature probably largely explain this observation. Nevertheless, regarding the potential rotation of a patient between two image acquisitions in routine clinical practice, the performance of the algorithm evaluated with a phantom study appeared to be highly adequate. Furthermore, the module which was used in this work to test the algorithm was the fully automatic one. With the advanced module, if required, users could probably improve the results by modifying parameters such as the value of the threshold to eliminate the noise in images, especially for PET images.

5. Conclusion

The present study showed that the block matching automatic registration algorithm was robust and reliable and yielded very satisfactory results for CT/CT and MR/CT registrations: the algorithm correctly handled the automatic registration of images with differences in rotation between phantom positions up to 40°. The algorithm's performance was also very good for PET/CT automatic registrations of images with differences in rotation between phantom positions up to 20 to 30°.

This study has made us confident about the use of this algorithm in clinical practice, even if the validation by an expert of each new registration is still required.

Acknowledgements

The authors thank Dr Claude Comtat, from the Image Acquisition and Processing group, Frédéric Joliot hospital facility, French Atomic Energy Commission, for welcoming us to his department in order to perform acquisitions of the head phantom on the Ecat Exact HR^{+} PET camera. The authors also acknowledge Dr Jean-Christophe Diaz, from the Dosisoft company, for his help and advice, and Lorna Saint Ange for editing.

This work was undertaken in the framework of the MAESTRO Integrated Project (IP CE503564) funded by the European Commission.

References

[1] Barnden L, Kwiatek R, Lau Y, Hutton B, Thurfjell L, Pile K, et al. Validation of fully automatic brain SPET to MR co-registration. Eur J Nucl Med 2000;27:147–54.
[2] Besl PJ, McKay ND. A Method for registration of 3D shapes. IEEE Trans Pattern Anal Mach Intell 1992:239–56.
[3] Bonniaud G, Isambert A, Dhermain F, Beaudré A, Ferreira I, Ricard M, et al. Image registration for radiation therapy: practical aspects and quality control. Cancer Radiother 2006;10:222–30.
[4] Ciernik IF, Dizendorf E, Baumert BG, Reiner B, Burger C, Davis JB, et al. Radiation treatment planning with an integrated positron emission and computer tomography (PET/CT): a feasibility study. Int J Radiat Oncol Biol Phys 2003;57:853–63.
[5] Eberl S, Kanno I, Fulton RR, Ryan A, Hutton BF, Fulham MJ. Automated interstudy image registration technique for SPECT and PET. J Nucl Med 1996;37:137–45.
[6] Emami B, Sethi A, Petruzzelli GJ. Influence of MRI on target volume delineation and IMRT planning in nasopharyngeal carcinoma. Int J Radiat Oncol Biol Phys 2003;57:481–8.
[7] Fraass B, Doppke K, Hunt M, Kutcher G, Starkschall G, Stern R, et al. American Association of Physicists in Medicine Radiation Therapy Committee Task Group 53: quality assurance for clinical radiotherapy treatment planning. Med Phys 1998;25:1773–829.
[8] Grosu AL, Lachner R, Wiedenmann N, Stärk S, Thamm R, Kneschaurek P, et al. Validation of a method for automatic image fusion (BrainLAB

System) of CT data and ^{11}C-methionine-PET data for stereotactic radiotherapy using a LINAC: first clinical experience. Int J Radiat Oncol Biol Phys 2003;56:1450–63.

[9] Holden M, Hill DL, Denton ER, Jarosz JM, Cox TC, Rohlfing T, et al. Voxel similarity measures for 3-D serial MR brain image registration. IEEE Trans Med Imaging 2000;19:94–102.

[10] International Atomic Energy Agency. Commissioning and quality assurance of computerized planning systems for radiation treatment of cancer. Technical report series n° 430. Vienna: IAEA; 2004.

[11] Kiebel SJ, Ashburner J, Poline JB, Friston KJ. MRI and PET coregistration – a cross validation of statistical parametric mapping and automatic image registration. Neuroimage 1997;5:271–9.

[12] Lavely WC, Scarfone C, Cevikalp H, Li R, Byrne DW, Cmelak AJ, et al. Phantom validation of coregistration of PET and CT for image-guided radiotherapy. Med Phys 2004;31:1083–92.

[13] Lefkopoulos D, Ferreira I, Isambert A, Le Péchoux C, Mornex F. Present and future of the image guided radiotherapy (IGRT) and its applications in lung cancer treatment. Cancer Radiother 2007;11:23–31.

[14] Li X, Zhang P, Brisman R, Kutcher G. Use of simulated annealing for optimization of alignment parameters in limited MRI acquisition volumes of the brain. Med Phys 2005;32:2363–70.

[15] Maintz JBA, Viergever MA. A survey of medical image registration. Med Image Anal 1998;2:1–36.

[16] Mijnheer B, Olszewska A, Fiorino C, Hartmann G, Knöös T, Rosenwald JC et al. ESTRO Booklet n° 7. Quality assurance of treatment planning systems, practicle examples for non-IMRT photon beams; 2004.

[17] Mutic S, Dempsey JF, Bosch WR, Low DA, Drzymala RE, Chao KS, et al. Multimodality image registration quality assurance for conformal three-dimensional treatment planning. Int J Radiat Oncol Biol Phys 2001;51:255–60.

[18] Nestle U, Kremp S, Grosu AL. Practical integration of [$^{(18)}$F]-FDG-PET and PET-CT in the planning of radiotherapy for non-small cell lung cancer (NSCLC): the technical basis, ICRU-target volumes, problems, perspectives. Radiother Oncol 2006;81:209–25.

[19] Newbold K, Partridge M, Cook G, Sohaib SA, Charles-Edwards E, Rhys-Evans P, et al. Advanced imaging applied to radiotherapy planning in head and neck cancer: a clinical review. Br J Radiol 2006;79:554–61.

[20] Nishioka T, Shiga T, Shirato H, Tsukamoto E, Tsuchiya K, Kato T, et al. Image fusion between 18FDG-PET and MRI/CT for radiotherapy planning of oropharyngeal and nasopharyngeal carcinomas. Int J Radiat Oncol Biol Phys 2002;53:1051–7.

[21] Ourselin S, Stefanescu R, Pennec X. Robust registration of multi-modal images: towards real-time clinical applications. In: Takeyoshi Dohi and Ron Kikinis, editors. Medical image computing and computer-assisted intervention (MICCAI'02). Vol 2489 of LNCS, Tokyo, Springer; 2002. p.140–7.

[22] Pappas IP, Styner M, Malik P, Remonda L, Caversaccio M. Automatic method to assess local CT-MR imaging registration accuracy on images of the head. Am J Neuroradiol 2005;26:137–44.

[23] Sarkar A, Santiago RJ, Smith R, Kassaee A. Comparison of manual vs. automated multimodality (CT-MRI) image registration for brain tumors. Med Dosim 2005;30:20–4.

[24] Scarfone C, Lavely WC, Cmelak AJ, Delbeke D, Martin WH, Billheimer D, et al. Prospective feasibility trial of radiotherapy target definition for head and neck cancer using 3-dimensional PET and CT imaging. J Nucl Med 2004;45:543–52.

[25] Turkington TG, Jaszczak RJ, Pelizzari CA, Harris CC, MacFall JR, Hoffman JM, et al. Accuracy of registration of PET, SPECT and MR images of a brain phantom. J Nucl Med 1993;34:1587–94.

[26] Vaylet F, Bonnichon A, Salles Y, Gontier E, Bonardel G, Lefloch H. Positron emission tomography using 18F-fluorodeoxyglucose in the management of nonsmall cell lung cancers in 2006. Cancer Radiother 2007;11: 16–22.

[27] West J, Fitzpatrick JM, Wang MY, Dawant BM, Maurer Jr CR, Kessler RM, et al. Comparison and evaluation of retrospective intermodality brain image registration techniques. J Comput Assist Tomogr 1997;21: 554–66.

[28] Wu TH, Wang JK, Lee JJ, Liu RS, Guo WY. An imaging co-registration system using novel non-invasive and non-radioactive external markers. Eur J Nucl Med Mol Imaging 2003;30:812–8.

[29] Yokoi T, Soma T, Shinohara H, Matsuda H. Accuracy and reproducibility of co-registration techniques based on mutual information and normalized mutual information for MRI and SPECT brain images. Ann Nucl Med 2004;18:659–67.